EPJ A direct
electronic only

Nuclear structure far off stability —Implications for nuclear astrophysics

H. Grawe[1,a], A. Blazhev[1,2], M. Górska[1], R. Grzywacz[3], H. Mach[4], and I. Mukha[1,5,6]

[1] GSI, Planckstr. 1, D-64291 Darmstadt, Germany
[2] University of Sofia, Sofia, Bulgaria
[3] Department of Physics and Astronomy, University of Tennessee, Knoxville, TN 37996, USA
[4] ISV, Uppsala University, Nyköping, Sweden
[5] RRC Kurchatov Institute, RU-123481 Moscow, Russia
[6] Katholieke Universiteit Leuven, Leuven, Belgium

Abstract. The single-particle structure and shell gap of ^{100}Sn as inferred from previous in-beam γ-ray spectroscopy has been confirmed in recent studies of seniority and spin-gap isomers by $\gamma\gamma$, $\beta\gamma$, $\beta p\gamma$, $p\gamma$ and $2p\gamma$ spectroscopy. The results for ^{94,95}Ag, ^{98}Cd and its $N = 50$ isotones ^{96}Pd and ^{94}Ru stress the importance of large-scale shell model calculations employing realistic interactions for the isomerism, np-nh excitations, seniority mixing and $E2$ polarisation of the ^{100}Sn core. The strong monopole interaction of the $\Delta l = 0, 1$ spin/isospin-flip partners $\pi g_{9/2}$-$\nu g_{7/2}$ along the $N = 50$ isotones and the $\pi f_{5/2}$-$\nu g_{9/2}$ pair of nucleons along the $Z = 28$ Ni isotopes are decisive for the evolution of the shell structure towards ^{100}Sn and ^{78}Ni. It can be traced back to the tensor force in the effective nucleon-nucleon interaction and provides a straightforward explanation for new shells in neutron-rich light nuclei, implying qualitative predictions for new $N = 32, 34$ subshells in Ca isotopes, persistence of the ^{78}Ni proton and neutron shell gaps and non-equivalence of the $g_{9/2}$ valence mirror Ni isotopes and $N = 50$ isotones. This is corroborated by recent experimental data on ^{56,58}Cr and $^{70-76}$Ni. The implication of monopole driven shell evolution for apparent spin-orbit splitting towards $N \gg Z$ and structure along the astrophysical r-path between $N = 50$ and $N = 82$ is discussed.

PACS. 21.60.Cs Shell model – 23.20.-g Electromagnetic transitions – 27.30.+t $16 \leq A \leq 68$ – 27.60.+j $78 \leq A \leq 132$ – 26.50.+x Nuclear physics aspects of the r-process

1 Introduction

The evolution of shell structure towards exotic nuclei with extreme isospin has become, and will be for the future, the major topic of experimental studies and the main challenge for realistic in-medium nucleon-nucleon (NN) interactions as used in large-scale shell model and mean field theory. Especially on the neutron-rich side of the Segré chart, where the drip line for $A \geq 80$ is far beyond reach for experiments, the understanding of the underlying shell driving mechanism is of key importance for astrophysics applications as, *e.g.*, the r-process. Two scenarios with differing experimental signature have been proposed to describe the shell structure of nuclei on the pathway towards large N/Z ratios. The first is based on the larger radial extension and a softer neutron potential. This shifts large-l orbitals upward in energy and reduces the spin-orbit (SO) splitting, which is proportional to the potential gradient, for nucleon orbitals probing the nuclear surface [1,2]. Thus for medium-heavy and heavy nuclei the harmonic oscillator (HO) unique-parity shells are restored. The changing shell structure evolves smoothly with A and N/Z and only large variations of these parameters as expected towards the neutron dripline will have substantial effects. The second scenario originates from the strong monopole shifts of selected shell model orbits which have been ascribed to the $\sigma\tau$ central and the tensor force of the NN interaction [3,4,5,6]. This will be discussed in sect. 3 and recent experimental evidence for monopole driven shell structure and apparent SO splitting from the $^{100-132}$Sn and ^{48}Ca to ^{78}Ni regions is presented in sects. 2 and 4. The application to r-path nuclei is discussed in a qualitative way in sect. 5.

[a] Conference presenter e-mail: h.grawe@gsi.de
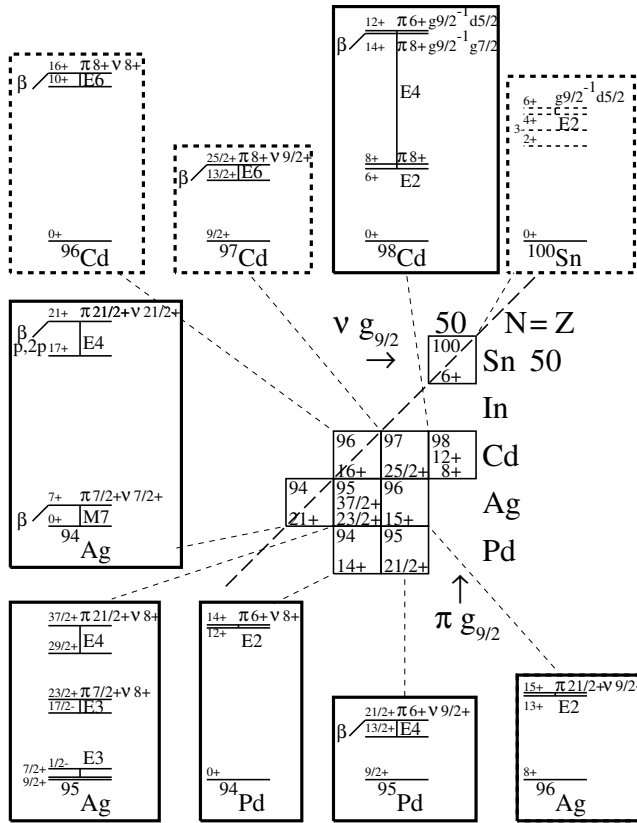
Fig. 1. Experimentally established (solid frames) and shell model predicted (dashed frames) spin-gap isomers close to ^{100}Sn.

2 Spin-gap isomerism in the ^{100}Sn region

In spite of the missing experimental information on binding energies and excited states in ^{100}Sn and its one-particle (hole) neighbours the shell structure as inferred from more remote nuclei by shell model aided extrapolation is well established [7,8,9]. It shows a remarkable similarity to ^{56}Ni one major shell below at $N = Z$ and close to the proton dripline. This implies the existence of analogous structure features such as softness with respect to $L = 2$ core excitations, a pronounced Gamow-Teller resonance due to the $\pi g_{9/2}$-$\nu g_{7/2}$ respective $\pi f_{7/2}$-$\nu f_{5/2}$ proton-neutron orbitals, a substantial amount of np-nh configurations besides the doubly-magic configuration in the ground state of ^{100}Sn, high-spin isomers, and possibly even proton decay. The study of seniority and spin-gap isomers provides a sensitive probe of single particle energies, residual interaction, core excitation and shell gaps as demonstrated in recent experiments on ^{98}Cd [10] and ^{94}Ag [11]. The status of observed isomers and shell model predicted ones and their main structure features in terms of the leading proton-neutron $g_{9/2}^n$ configuration are summarised in fig. 1. Besides the well known isomers ^{96}Ag, $I^\pi = (15^+)$ [12], ^{94}Pd, $I^\pi = 14^+$ [13] and ^{95}Pd, $I^\pi = 21/2^+$ [14,15], recently the cases of ^{95}Ag, $I^\pi = (23/2^+)$ and $I^\pi = (37/2^+)$ [16] were reported between the $N = 50$ and the $N = Z$ lines below ^{100}Sn.
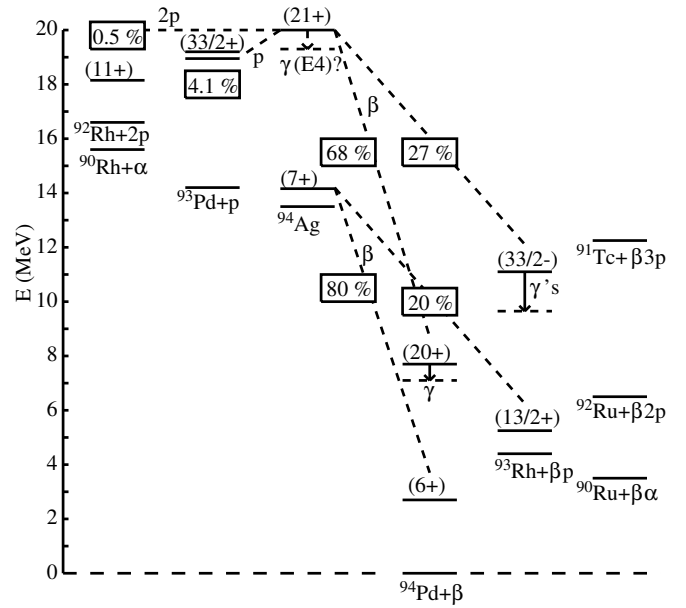
Fig. 2. Decay channels for the $I^\pi = (21^+)$ isomer in ^{94}Ag.

The spin-gap isomers with the highest spins, as, *e.g.*, the $I^\pi = (37/2)^+$ state in ^{95}Ag, which exhaust the $\pi\nu g_{9/2}^n$ configuration, are not predicted to be isomeric in the proton-neutron $(p_{1/2}, g_{9/2})$ valence space [17] and require excitation of the ^{100}Sn core. This has been studied recently in a dedicated prompt-delayed experiment at the EUROBALL IV array, where the $I^\pi = (12^+)$ core excited isomer in ^{98}Cd, the two-proton hole neighbour of ^{100}Sn, was identified [10]. The decay pattern exhibits a striking analogy to ^{54}Fe, two proton holes from ^{56}Ni [9,18]. The level scheme, the core excited isomer and the $E2$ transition rates are excellently reproduced by a large scale shell model (LSSM) calculation in the $(0g, 1d, 2s)$ model space allowing for up to $4p4h$ excitations of the ^{100}Sn core. Values of 6.46 (15) MeV for the ^{100}Sn shell gap were inferred from the excitation energy of the $I^\pi = (12^+)$ $E4$ isomer, and a small proton polarisation charge of $\delta e_\pi \leq 0.2e$ was extracted from the $\pi g_{9/2}^{-2}$; $I^\pi = (8^+)$ $E2$ isomeric decay [10,19]. It should be noted that the LSSM, which exhibits good predictive power for isomers and $E2$ strengths in the whole region between $N = 50$ and the $N = Z$ line (see below ^{94}Ag and sect. 4.2), also predicts an $I^\pi = 14^+$ $E6$ isomer in ^{98}Cd and an $I^\pi = 6^+$ $E2$ isomer in ^{100}Sn. Like the $I^\pi = 25/2^+$ and 16^+ $E6$ isomers in ^{97,96}Cd, which are expected [17] and searched for since long, they await future experimental verification (fig. 1).

A second example for the sensitivity of spin-gap isomers to subtle structure details such as single particle energies, shell gaps and proton-neutron $(\pi\nu)$ interaction even in LSSM calculations is provided by the $I^\pi = (21^+)$ isomer in ^{94}Ag. This state features exotic properties with respect to spin, excitation energy and decay modes (fig. 2) to a degree, which is unprecedented in the Segré chart [11, 20,21,22]. The isomerism is not predicted in the pure valence hole space below ^{100}Sn but requires inclusion of
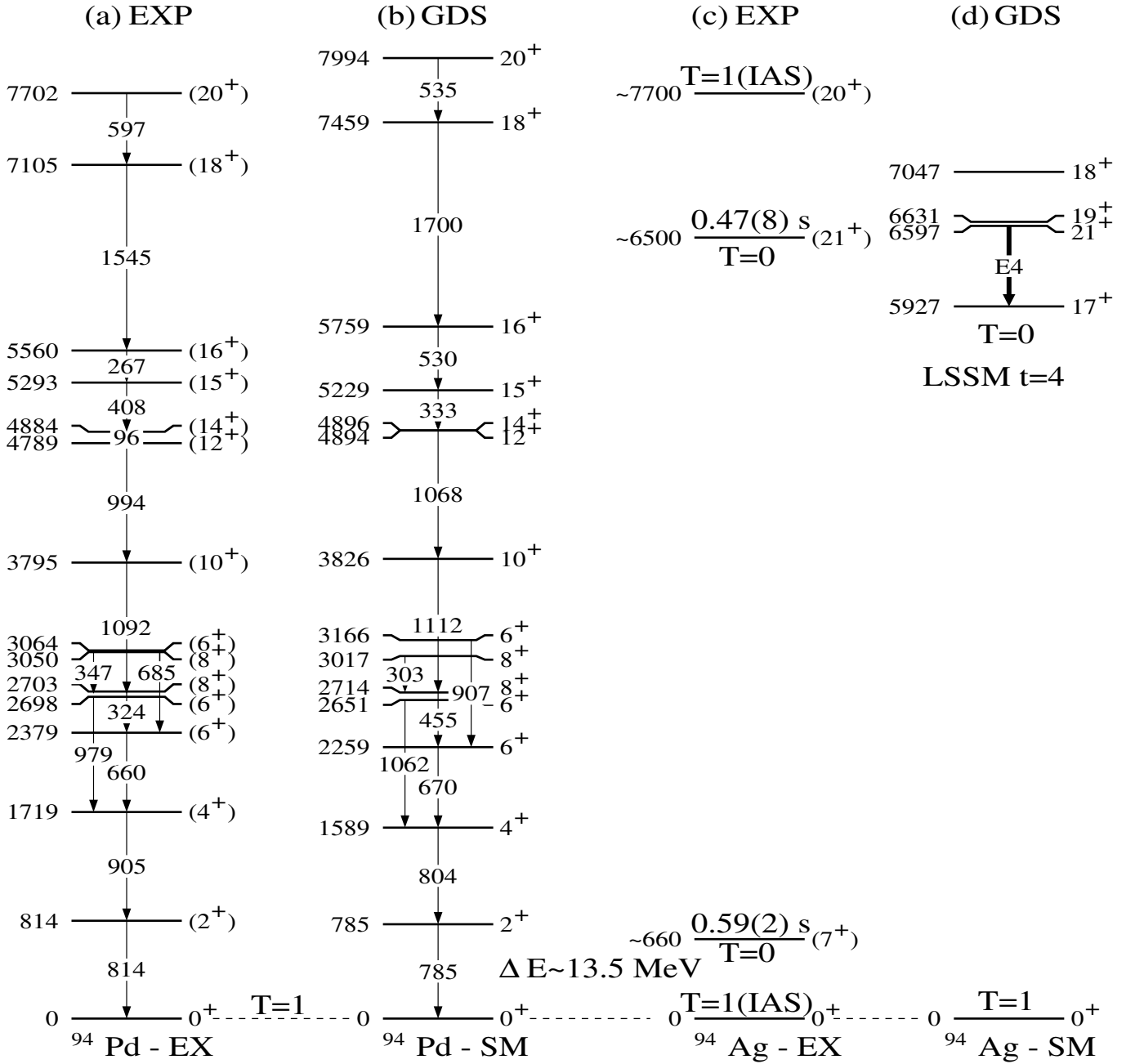
Fig. 3. Experimental and large-scale shell model level scheme for ^{94}Ag and its $\beta\gamma$ daughter ^{94}Pd. The $T = 0$ states in ^{94}Ag are normalised to the $T = 1$ isobaric analogue states (IAS).

core excitations in the $(0g, 1d, 2s)$ model space. Excellent agreement between LSSM calculations and experiment is observed without any specific modification of the LSSM input used in the $N = 50$ to $N = Z$ region. The quality of agreement is demonstrated in fig. 3 for the $T = 1$ daughter states in ^{94}Pd populated in the $\beta\gamma$ decay of the $I^\pi = (21^+)$ and 7^+ isomers [11]. The decay scheme of the high-spin state as shown in fig. 2 allows for a number of different and due to the high-excitation energy and spin quite exotic decay modes, which were observed in follow-up experiments as $\beta\gamma$ [11], $\beta p\gamma$ [20], $p\gamma$ [21], $2p\gamma$ [22] channels. It should be emphasised that detection of the exotic decay modes

was only due to the high spin of the isomer which enabled application of high-spin γ-decay spectroscopy via $p\gamma\gamma$ and $2p\gamma\gamma$ coincidence techniques [21, 22]. Properties and decay modes of the isomer can be summarised as follows:

– highest spin (21^+) and energy $(6.5\,\text{MeV})$ of a β decaying isomer in the Segré chart;
– spin-gap isomer with maximum aligned proton and neutron spin and leading configuration $(\pi g_{9/2}^{-3})_{21/2}\,(\nu g_{9/2}^{-3})_{21/2}$;
– isomerism reproduced in LSSM including $4p4h$ excitations of the ^{100}Sn core;

- one-proton emitter ($l = 4, 6$) with extremely small spectroscopic factor ($< 10^{-5}$ for $l = 4$);
- correlated two-proton emission dominates as sequential decay is hindered by small spectroscopic factor and large γ-decay widths;
- two-proton width largely enhanced due to a highly deformed shape isomer.

It is obvious that the characteristics of the one-proton and correlated two-proton emission are beyond the scope of even the LSSM calculations. Nevertheless in the simplest valence hole space the spectroscopic factor for $l = 4$ proton emission is only 4% and the quadrupole moment of the parent state is larger by more than a factor of two relative to the daughter. It should be noted that the high-spin isomers $I^\pi = (37/2^+)$ in ^{95}Ag and $I^\pi = (12^+, 14^+)$ in ^{98}Cd are further candidates for direct proton emission.

The success of the shell model in the description of the high-spin isomerism is due to the fact that the $\pi\nu$ realistic interaction is well tuned for the model space and gives a correct description of the evolution of single-particle energies. In fig. 4 the extrapolation of single neutron energies from experimentally known values in ^{88}Sr respective ^{90}Zr to ^{100}Sn is shown for two different realistic interactions GG [23] and MHJ [24]. The agreement with experimentally identified single-neutron states in $N = 51$ nuclei and among the two interactions demonstrates the reliability of this shell model aided extrapolation. The deviations as, e.g., the $d_{5/2}$-$g_{7/2}$ inversion in ^{101}Sn show the systematic uncertainty of the procedure, which in this specific case is due to an improper $\pi g_{9/2}\nu g_{7/2}$ monopole in the MHJ interaction, which will be further discussed in sect. 5.

It is the monopole part of the $\pi\nu$ interaction that determines the evolution of the neutron single particle (hole) energies and the $N = 50$ shell gap upon filling of the $\pi 0g_{9/2}$ orbit from the experimentally known $Z = 40$ region towards $Z = 50$ (fig. 4). The monopole for a specific multiplet (j, j') is defined by

$$V_{jj'}^m = \sum_J (2J+1)\langle jj'J |V| jj'J\rangle / \sum_J (2J+1), \quad (1)$$

which gives rise to the single-particle energy evolution between two shell closures CS and CS' [9]

$$\epsilon_j^{CS} = \epsilon_j^{CS'} + \sum_{j'} (2j' + 1 - \delta_{jj'}) V_{jj'}^m . \quad (2)$$

The Kronecker symbol applies for $T = 1$ and identical orbitals to maintain the Pauli principle. This simple formula can be used to calculate the single particle energies for ^{100}Sn from the experimentally known ones in ^{90}Zr or ^{88}Sr as shown in fig. 4 for neutrons and a given residual interaction. It should be noted that eq. (2) holds only for closed j' shells, i.e. in the example of fig. 4 ($j' = \pi g_{9/2}$) for ^{90}Zr and ^{100}Sn, in between due to configuration mixing the trend deviates from a strict scaling with the $j' = \pi g_{9/2}$ occupation and the exact progression can be inferred from a full shell model calculation (see fig. 4). In fig. 4 the spin-flip pairs $\pi 0g_{9/2}\nu 0g_{7/2}$, which are also spin-orbit partners ($\Delta l = 0$), and $\pi 0g_{9/2}\nu 1d_{3/2}$ ($\Delta l = 2$) exhibit much
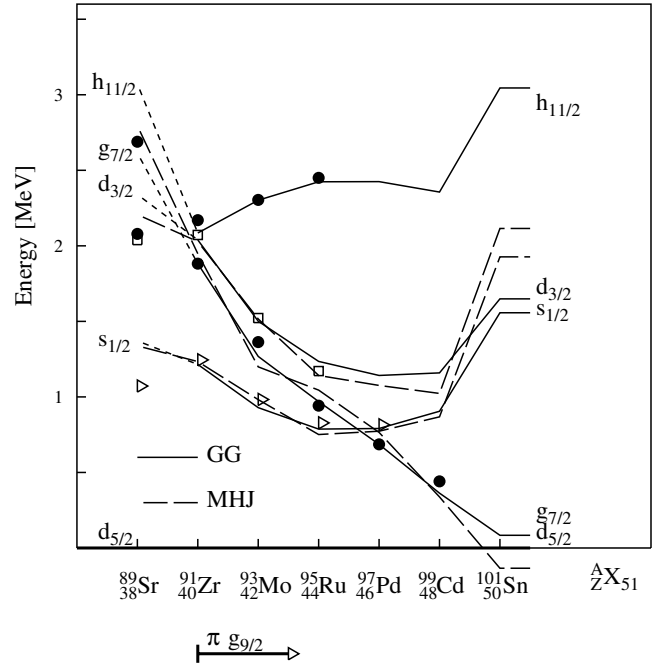
Fig. 4. Evolution of $N = 51$ single-particle energies relative to the $\nu d_{5/2}$ ground state for two different realistic interactions (GG) [23] and (MHJ) [24].

larger downward steps from ^{90}Zr to ^{100}Sn as compared to the $\nu 1d_{5/2}$ reference state, i.e. comparatively larger monopoles. This is a very general feature of the $\pi\nu$ interaction which is especially strong when the corresponding radial wave functions have good overlap [5,9] (see sect. 3). We also note that the evolution of neutron single-particle energies from ^{90}Zr ($Z = 40$) to ^{100}Sn ($Z = 50$) and single hole energies from ^{132}Sn to ^{122}Zr is described by the same interaction only slightly modified due to the different core mass (see sect. 5).

3 Monopole driven shell structure in neutron-rich nuclei

Strong monopole drifts are not restricted to the examples shown in fig. 4 but have been experimentally observed all over the Segré chart, the most prominent being the $\Delta l = 0$ spin-orbit $\pi\nu$ pairs $0p_{3/2}$-$0p_{1/2}$, $0d_{5/2}$-$0d_{3/2}$, $0f_{7/2}$-$0f_{5/2}$, $0g_{9/2}$-$0g_{7/2}$ and the $\Delta l = 1$ spin-flip pairs $0p_{1/2}$-$0d_{5/2}$, $0d_{3/2}$-$0f_{7/2}$, $0f_{5/2}$-$0g_{9/2}$, $0g_{7/2}$-$0h_{11/2}$. They are summarised in recent reviews [3,5,9,25] and can be traced back to the $\sigma\tau$ and tensor parts of the NN interaction [3, 4]. The empirical evidence translates into the following criteria for strong monopoles: i) the interacting nucleons are spin-flip partners with ii) $\Delta l = 0, 1, 2$ and iii) should have the same number of nodes in their radial wave functions to optimize the overlap. These features are also borne out in realistic interactions as derived from effective NN potentials fitted to scattering data via standard many-body techniques [24] as shown in fig. 17 of [9]. They suffer, however, from the fact that due to the neglect of three-body

Tensor force acting on spin-isospin flip nucleons ($j_>\, j'_<$, $\pi\,\nu$)

light nuclei :	medium-heavy nuclei :
new neutron shells along isotone chains	proton shell reordering along isotope chains

$V = - |v_{\sigma\tau}(r)| \, (\tau_1 \cdot \tau_2)\,(\sigma_1 \cdot \sigma_2)$ $\Leftrightarrow$ $V = - |v_T\,(r)| \, (\tau_1 \cdot \tau_2)\,([\sigma_1 \cdot \sigma_2]^{(2)}Y^{(2)}(\Omega))$

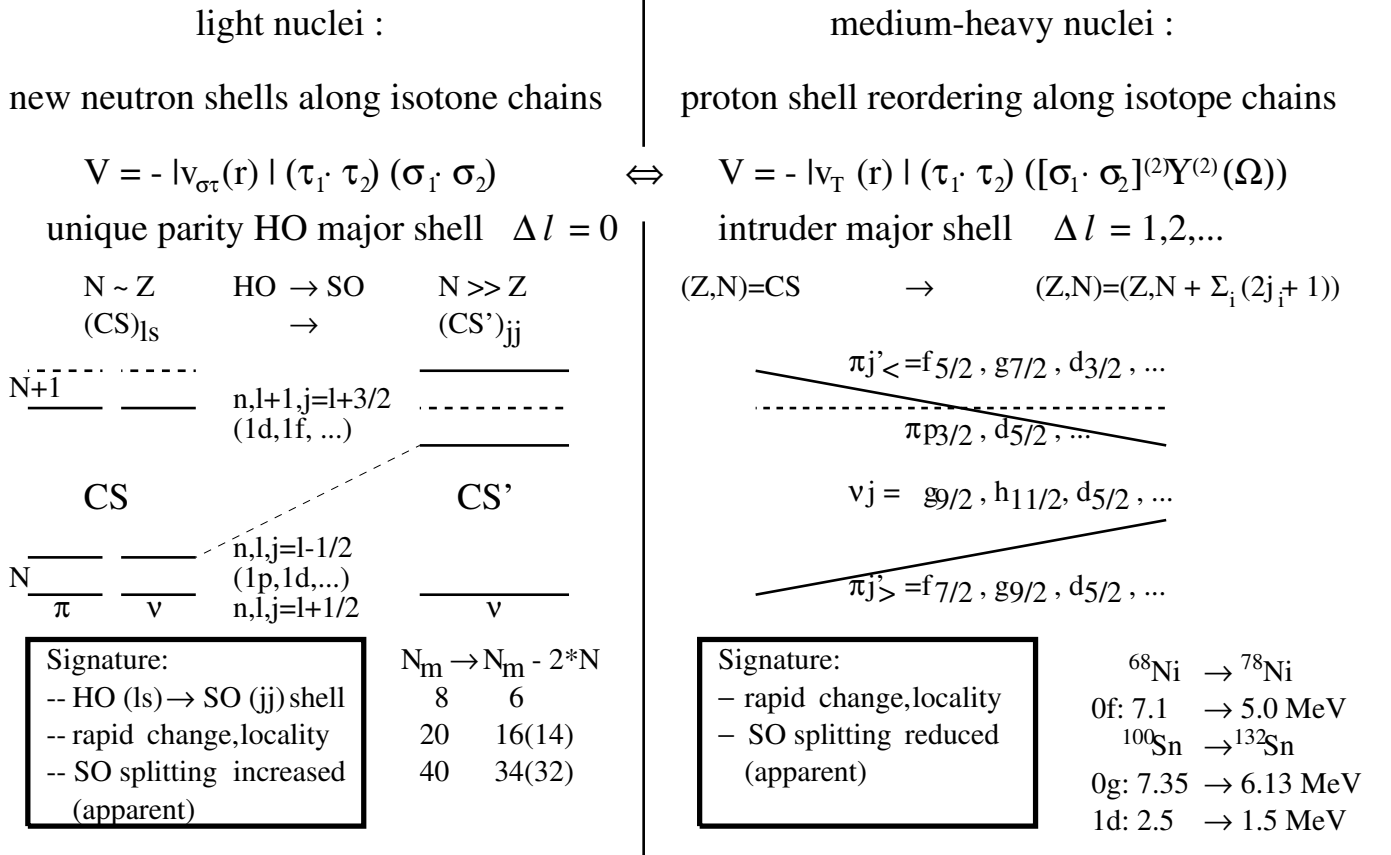| unique parity HO major shell $\Delta l = 0$	intruder major shell $\Delta l = 1,2,...$

Fig. 5. Schematic illustration of signatures for tensor force driven shell evolution.

effects the monopole part is not determined well and has to be tuned to experimental shell evolution, which hampers their predictive power. The dramatic impact of monopole drifts and the sensitivity to subtle details of the interaction is due to the factor $(2j'+1)$ in eq. (2) which is large in filling (emptying) a high-spin orbital j' and translates monopole corrections of about $100\,\mathrm{keV}$ into MeV.

On the NN interaction level the strong monopoles are due to the tensor force

$$V = -|v_T(r)|(\tau_1 \cdot \tau_2)([\sigma_1 \cdot \sigma_2]^{(2)}Y^{(2)}(\Omega)), \qquad (3)$$

which can be shown to reduce within a unique parity harmonic oscillator shell to [4] to the central $\sigma\tau$ force

$$V = -|v_{\sigma\tau}(r)|(\tau_1 \cdot \tau_2)(\sigma_1 \cdot \sigma_2) \qquad (4)$$

3.1 New shells in light nuclei and shell reordering in medium-heavy nuclei

In fig. 5 the shell driving signatures of these interactions are compared schematically.

– In light nuclei within unique harmonic-oscillator shells starting with an ls-closed $N = Z$ doubly magic nucleus as ^{16}O or ^{40}Ca and proceeding towards $N \gg Z$ along

an isotonic chain by proton removal the HO magic neutron number N_m is changed to $N_m - 2 \cdot N$, where N is the HO principal quantum number. This is due to the fact that upon emptying the $\pi j = l + 1/2$ orbit the $\nu j = l - 1/2$ becomes less bound due to the strong $\Delta l = 0$ (spin-orbit partners) $\sigma\tau$ monopole. Before the empty $\pi j = l - 1/2$ orbit releases the $\nu j' = l + 1 - 1/2$ orbit of the adjacent shell by action of the tensor $\Delta l = 1$ (spin-flip) monopole and stabilises the N_m neutron shell for $Z = N_m - 2 \cdot N$ as observed in ^{14}C, ^{36}S and ^{34}S, which demonstrates the isospin symmetry of the scenario. This converts an ls closed shell $N_m = 8$ (^{16}O), 20 (^{40}Ca), 40 (^{68}Ni) into jj closures $N'_m = 6, (14)16, (32)34$. The ambiguity is due to the presence of a $j = 1/2$ shell which exhibits a strong $T = 1$, $J = 0$ pairing matrix element (identical with the monopole for $j = 1/2$), and thus opens another gap upon filling or emptying this orbit. The scenario shown on the left side of fig. 5 gives rise to a new shell closure chart as shown in refs. [5,6,9]. Simultaneously the isotones in the HO oscillator semi-magic nuclei due the shell quenching and particle-hole excitations across the shell develop deformation as observed in ^{12}Be (fig. 20 in ref. [9]), ^{32}Mg [26] and ^{66}Fe [27]. Further abundant experimental evidence is presented in refs. [3,5,6,9].
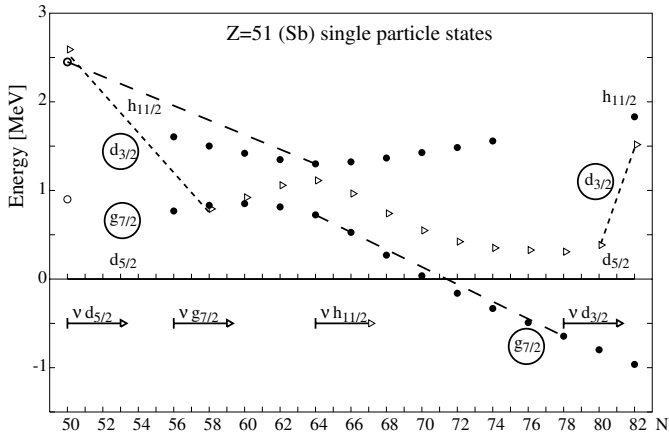
Fig. 6. Apparent spin-orbit splitting for $Z = 51$ single proton orbitals with reference to the $\pi d_{5/2}$ state. Experimental values are denoted by full circles, extrapolated ones by open circles. Dashed lines are drawn to guide the eye.

– In medium-heavy nuclei starting from a jj-closed doubly magic nucleus as ^{68}Ni or ^{100}Sn and going neutron-rich along an isotopic (Ni or Sn) chain by adding neutrons the apparent spin-orbit splitting of proton $\pi j = l \pm 1/2$ orbits is reduced when filling the $\nu j = l+1+1/2$ due to the $\Delta l = 1$ tensor monopole. It can be shown that the following identity holds [4]:

$$(2j_> + 1)V^m_{j'j_>} + (2j_< + 1)V^m_{j'j_<} = 0 \qquad (5)$$

for $T = 0, 1$, *i.e.* for $\pi\nu$, where in the present scenario j' is a neutron orbit and $(j_>, j_<)$ denote proton levels or vice versa as it is again symmetric in isospin. The shell evolution is schematically illustrated on the right side of fig. 5. Representative experimental numbers are given for the $Z = 28$ (Ni) and $Z = 50$ (Sn) proton levels in fig. 5. It should be noted that the values for ^{78}Ni and ^{100}Sn have been extrapolated by shell model aided extrapolation assuming realistic interactions. As for heavier nuclei the spin-orbit force increases so much that it does not determine the shell gap alone, in spite of the SO split reduction by the tensor force the shell gap is only reduced but not fully quenched. The effect is experimentally well established as shown in fig. 16 b,c of ref. [9] and in fig. 6 below for the $\nu g_{9/2}\pi f$ and the $\nu h_{11/2}\pi g$. This will be further discussed in sects. 4 and 5.

3.2 Apparent spin-orbit splitting driven by monopole shift

The signatures listed in fig. 5 and with respect to SO splitting may be compared to the scenario described in the introduction (sect. 1). They are not restricted to neutron-rich nuclei as they are symmetric in isospin, *i.e.* they hold for exchange of protons and neutrons though their importance to proton-rich nuclei is limited due to the close-lying

dripline. The sign of the change in SO splitting reverses upon filling/emptying of an orbit. It is in contrast for the shell quenching scenario described in sect. 1 i) not determined by the gradient in N/Z ratio and ii) not restricted to neutron orbits. This is illustrated in fig. 6 for the $Z = 51$ (Sb) single particle states when filling the major neutron shell from ^{100}Sn to ^{132}Sn. In the following qualitative discussion it should be kept in mind that the neutron orbitals are not filled successively but due to configuration mixing partly in parallel, and that spectroscopic factors have been measured consistently only for the $\pi g_{7/2}$ and $\pi h_{11/2}$ states [28]. Striking monopole drifts can be observed for the $\pi\nu g_{7/2}$-$h_{11/2}$ and the $\pi\nu d_{3/2}$-$d_{5/2}$ pair of nucleons.

– It is known since long that the $\pi g_{7/2}$ is more strongly bound relative to the $\pi d_{5/2}$ reference state as soon as the $\nu h_{11/2}$ is filled above $N = 64$ with a net effect of ~ 1.9 MeV. The same monopole determines the downsloping of the $\pi h_{11/2}$ upon filling of the $\nu g_{7/2}$ between $N = 50$ and 64 by ~ 1.2 MeV. The ratio of the net effects according to eq. (2) is close to that of the multiplicities $(2j+1)$ of the filled neutron orbitals, namely 12/8. The exact trend is distorted in this case as the $\nu g_{7/2}$ is also acting on the $\pi d_{5/2}$ reference state. From eq. (5) one would expect that the $\pi g_{9/2}$ spin-orbit partner would be lifted up by filling of the $\nu h_{11/2}$ which should result in a reduced πg SO splitting. The latter effect is masked and compensated, however, by the strong (see fig. 4) $\pi g_{9/2}$-$\nu g_{7/2}$ monopole, as the $\nu g_{7/2}$ is filled before and/or in parallel.
– With respect to apparent spin-orbit splitting the $\pi d_{3/2}$-$d_{5/2}$ distance is a much better study object. The splitting reduces from $N = 50$ to 56 when the $\nu d_{5/2}$ orbit is filled, it increases from $N = 78$ to 82 when the filling of the $\nu d_{3/2}$ binds the reference level $\pi d_{5/2}$ more strongly than the $\pi d_{3/2}$. As it is the identical monopole which rules the shift, the ratio of down- and up-shift should be 4/6. In fact the ratio is smaller and this is due to two other neutron orbitals that are being filled in between. From $N = 56$ to 64 the splitting increases due to the $\nu g_{7/2}$ filling effect on the $\pi d_{5/2}$ reference while from $N = 64$ to 76 it reduces again due to the $\pi d_{3/2}$-$\nu h_{11/2}$ monopole. Again the multiplicity factor 12/8 results in a net decrease of the SO splitting, if the two different monopoles involved have a similar value.

As the sign of the SO splitting always places the $j_<$ level above the $j_>$ it can be concluded that a major part of the observed SO reduction for proton levels by adding neutrons from $N = Z$ towards larger N/Z values within a full major shell is related to the trivial $(2j+1)$ weighting factor of eq. (2) that always favours $j_<$ over $j_>$ energetically as discussed for proton states along the Sn isotopes. The opposite holds for neutron levels when protons are removed towards larger N/Z along isotonic chains. This is not in contradiction to the recently observed SO reduction along $N = 82$ from ^{144}Sm to ^{132}Sn [28], as this covers only the lowest $\pi 1d_{5/2}$ and $\pi 0g_{7/2}$ part of the $Z = 50$–82 proton shell leaving aside the effect by the $\pi 1d_{3/2}$ and $\pi 0h_{11/2}$ orbitals.

4 Towards ^{78}Ni

4.1 From ^{48}Ca to ^{78}Ni

The heaviest nucleus with doubly-magic features and an *ls*-closed HO neutron shell is ^{68}Ni at $N = 40$. The neutron shell gap has been discussed in many publications and was found to be small and to disappear at more than two nucleons distance from ^{68}Ni [9,27,29,30]. This can be understood within the framework of the scenarios shown in sect. 3 and fig. 5. Towards the neutron-rich Ca isotopes the removal of $\pi f_{7/2}$ protons will release the $\nu f_{5/2}$ neutrons to close the $N = 40$ gap. Experimentally deformation was observed already in ^{66,67}Fe [27,31] and ^{64}Cr would correspond to ^{32}Mg one major shell lower. The $N = 40$ gap according to this scenario would shift to $N = 32, 34$ in the Ca isotopes. Recently relativistic Coulomb excitation experiments were performed on the $N = 32, 34$ Cr [32] and Ti [33] isotopes. In both cases clear evidence for a $N = 32$ subshell was observed in the $B(E2, 2^+ \rightarrow 0^+)$ transition strength, which corroborates an earlier conclusion from excited states in ^{54}Ti [34]. On the other hand evidence for the $N = 34$ closure was not seen and it may develop only in the Ca isotopes.

Beyond ^{68}Ni the doubly-magic $N = 50$ nucleus ^{78}Ni has been the subject of numerous experimental studies with respect to the persistence of the $N = 50$ shell and its relevance for the astrophysics r-path. Early β-decay results seem to indicate a substantial shell quenching [35], while in-beam experiments on $N \sim 50$ Ge-Se isotopes [36] and isomer studies following fragmentation [37,38,39,40] give evidence for the persistence of the $N = 50$ shell. Decisive for both the $Z = 28$ and $N = 50$ shell gaps in ^{78}Ni is according to the tensor force scenario sketched on the right hand side of fig. 5 the monopole part of the spin-flip $\Delta l = 1$ $\pi 0 f_{5/2} \nu 0 g_{9/2}$ pair of nucleons. In Ni isotopes ($Z = 28$) beyond $N = 40$ by filling of the $\nu 0 g_{9/2}$ shell the $\pi 0 f_{5/2}$ orbit is bound more strongly than the adjacent $\pi 1 p_{3/2}$ and $\pi 0 f_{7/2}$ and eventually crosses the $\pi 1 p_{3/2}$ to enter the shell gap. This was experimentally observed up to $N = 44$ in the β decay of odd-A Ni isotopes [41]. Governed by the same monopole, along $N = 50$ the removal of $\pi 0 f_{5/2}$ protons will release the $\nu 0 g_{9/2}$ stronger than $\nu 1 d_{5/2}$ which will reduce the gap. Recent shell model extrapolations of the $Z = 28$ and $N = 50$ shell gaps from ^{68}Ni and ^{90}Zr, respectively, to ^{78}Ni yielded persistence of the proton and neutron shell gaps with ~ 5.1 MeV (see fig. 5) and ~ 3.5 MeV, respectively [6]. This is in agreement with experimental evidence on the persistence of $\nu 0 g_{9/2}^2$ seniority isomerism from $N = 42$ (^{70}Ni) to $N = 48$ (^{78}Zn, ^{76}Ni) [37,38,39,40] and the $N = 50$ shell strength in Ge isotopes [36]. The inferred ^{78}Ni shell gaps along with the recently determined empirical $T = 1$ interaction and single particle (hole) energies for the $N = 50$ isotones and Ni isotopes [42] provide a new bench mark for tuning the monopole interaction in the ^{48}Ca to ^{78}Ni model space. In the lower right panel of fig. 7 the experimental $E2$ strengths $B(E2; 8^+ \rightarrow 6^+)$ in the Ni isotopes beyond $N = 40$ are compared to recent shell model results in the full $(0f_{5/2}, 1p, 0g_{9/2})$ model space [42]. The shell model accounts very well for the observed $E2$ strength and the disappearance of the $I^\pi = 8^+$ isomerism in ^{72,74}Ni [43,44], which is intimately connected to the low $I^\pi = 2^+$ excitation energies [9,43], *i.e.* a strongly bound $\nu g_{9/2}^2; I^\pi = 2^+$ two-body matrix element. As a consequence in the $\nu g_{9/2}^n$ multiplet for $n = 4, 6$ the seniority $v = 4$ are more strongly bound which opens a new $8^+, v = 2 \rightarrow 6^+, v = 4$ $\Delta v = 2$ decay channel with a large $E2$ strength as shown in fig. 7, lower right panel. The microscopic origin of the low $I^\pi = 2^+$ excitation energy, which is experimentally verified in $^{70-76}$Ni [37,44,40], can be ascribed to a reduction of the $\pi 0 f$ SO splitting and the $Z = 28$ shell gap due to the strong tensor force $\nu g_{9/2} \pi f$ monopole as discussed in sect. 3 and fig. 5 [4]. The deviation of the $E2$ trend in the heavy Ni isotopes from their $N = 50$ valence mirror nuclei will be discussed in sect. 4.2.

4.2 Valence mirrors and break-down of the seniority scheme

In fig. 7 experimental and shell model $E2$ transition strengths for the $N > 40$ even Ni isotopes are compared to their $g_{9/2}^n$ valence mirror $N = 50$ isotones. Shell model calculations were performed with a new empirical interaction in the full $T = 1$ $(0f_{5/2}, 1p, 0g_{9/2})$ neutron respective proton model space [42]. The conclusions from the comparison in fig. 7 can be summarised as follows:

- The $B(E2)$ values for the yrast states do not show any mirror symmetry in the $n = 4, 6$ midshell nuclei. Nevertheless the $v = 2, 4$ states in the Ni isotopes have good seniority.
- The agreement for $\Delta v = 0$ transitions of yrast states is excellent.
- The $B(E2; 2^+ \rightarrow 0^+)$ in ^{70}Ni is largely underestimated in the shell model [45]. This is further evidence that the $Z = 28$ shell gap is soft against proton core excitation due to a monopole driven shell quenching (see sect. 4.1). As the $N = 50$ isotones have different neutron shell structure the valence mirror ^{92}Mo is affected only marginally by core excitation (upper left panel in fig. 7).
- The $B(E2; 4^+ \rightarrow 2^+)$ in the $n = 4, 6$ $N = 50$ isotones ^{94}Ru and ^{96}Pd cannot be reproduced in the $T = 1$ shell model approach [46]. It can be shown that this is a general feature of all calculations in a pure proton space [47]. On the other hand the large scale shell model as described in sect. 2 without further modification can describe these transitions if up to $4p4h$ excitations across $N = 50$ are included (dashed line in fig. 7). The core excitations mix proton and neutrons and hence cause the breakdown of the seniority scheme by mixing $v = 2, 4$ configurations in the $I^\pi = 4^+$ state [47].

5 Shell structure along the r-path towards $N \gg Z$

The success of the concept of monopole driven shell structure especially for the partially quenched $N = 50$ shell
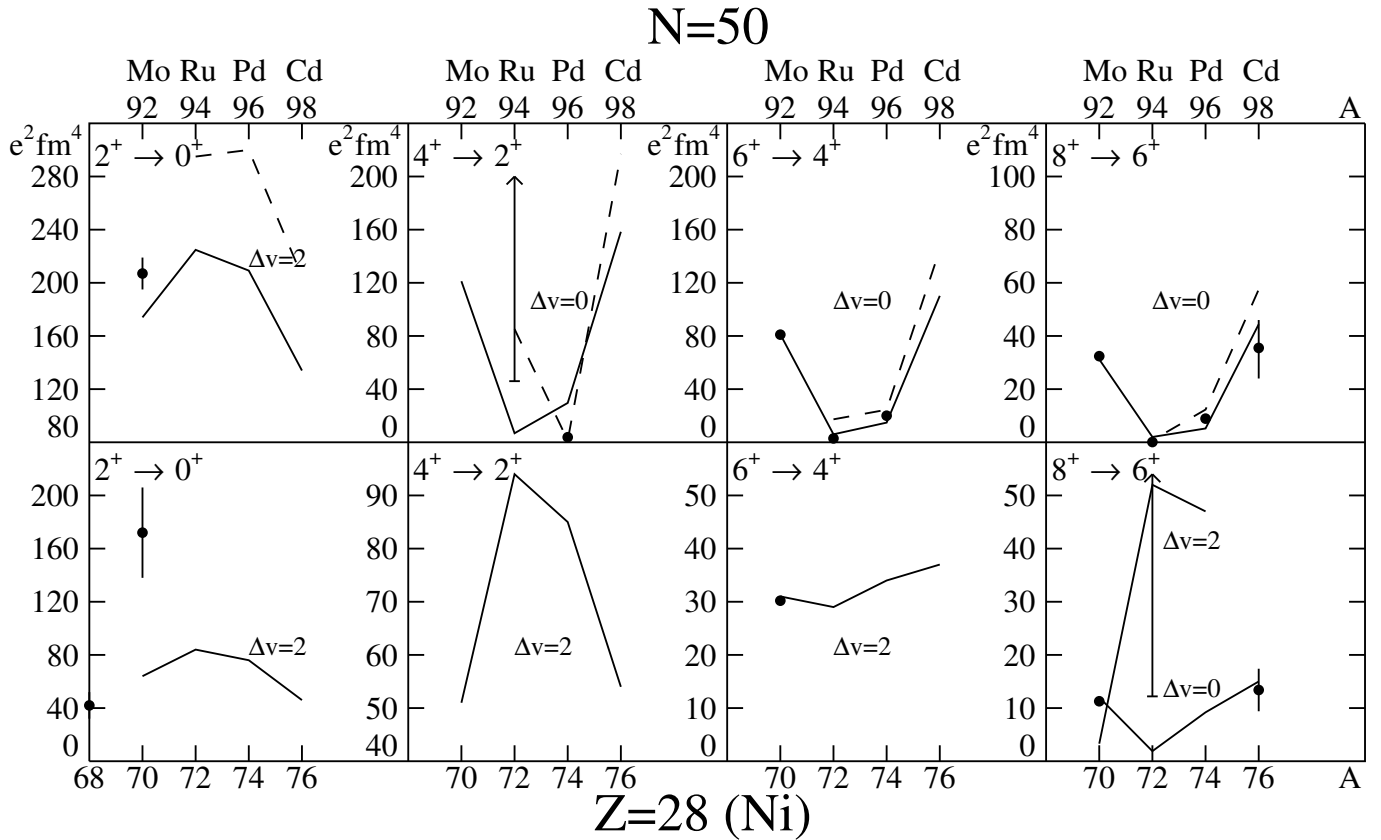
Fig. 7. $E2$ transition strengths within the $g_{9/2}^n$ configuration in even Ni isotopes (lower panel) and the $N = 50$ valence mirror partners (upper panel).

at ^{78}Ni, raises the question whether this could provide a possible scenario to understand the r-path abundance deficiency trough below the $A \simeq 130$ peak in astrophysical network calculations [48]. Quenching of the $N = 82$ shell due to a softening of the neutron potential as described in the introduction [2] has been invoked to explain this abundance deficiency [48] and experimental evidence for a reduced shell gap for $N = 82$, $Z \le 50$ has been presented [49,50]. While the nuclear structure origin of the astrophysics problem is still controversial, it might be appropriate to also look into alternative structure scenarios. In essence a reduced $N = 82$ shell gap causes increased excitation of neutrons into orbitals beyond $N = 82$ leading eventually to deformation. As a consequence the β-decay halflives at the previous waiting points become shorter due to larger Q_β values while they are increased for smaller neutron numbers due to the delayed filling of the $\nu 0g_{7/2}$ subshell which is the key orbital for the $\nu 0g_{7/2} \rightarrow \nu 0g_{9/2}$ allowed Gamow-Teller (GT) transition.

The relevant r-path nuclei are found below ^{132}Sn at $Z \le 50$ with the single neutron states playing the key rôle. The evolution of the neutron hole states is governed by the same $\pi 0g_{9/2}\nu j$ interaction [24] as for the neutron particles along $N = 50$ as shown in fig. 4 (MHJ) except for a renormalisation due to the different shell model core, which in the simplest case is an $A^{-1/3}$ scaling. In the left

panel of fig. 8 the evolution of the $N = 51$ neutron levels according to eq. (2) is shown with this interaction. The right panel shows the evolution of the $N = 81$ neutron hole states with an interaction as determined for a ^{132}Sn core [6,24]. Starting points are the experimental values adopted for ^{132}Sn [8,9]. It should be noted that eq. (2) holds only for closed j' shells, i.e. in the example of fig. 8 for the points, provided the proton shell gap is preserved, too. In between due to configuration mixing the trend may deviate from the lines drawn to guide the eye. The exact progression can be inferred from a full shell model calculation (see fig. 4 for the $N = 51$ case). This does not exclude a shell gap reduction due to cross shell excitations when moving away from a doubly-magic nucleus along a semi-magic chain of nuclei. Note that, e.g., from ^{100}Sn to ^{94}Ru this amounts to a ~ 2 MeV reduction.

To validate this extrapolation it has to be proven that the $Z = 40$ gap is preserved for ^{122}Zr. In the upper panel of fig. 9 the evolution of the $Z = 40$ gap and the adjacent single proton levels from $N = 50$ to 82 is shown. The realistic interaction based on the CD Bonn potential is identical with the one denoted by MHJ in fig. 4, derived for a ^{88}Sr core [24]. The results according to eq. (2) are drawn by dashed lines. It is obvious that the experimental points known until $N = 64$ are not well reproduced. The interaction fails in two details: i) it reverses the $\nu 0g_{7/2}$-$1d_{5/2}$
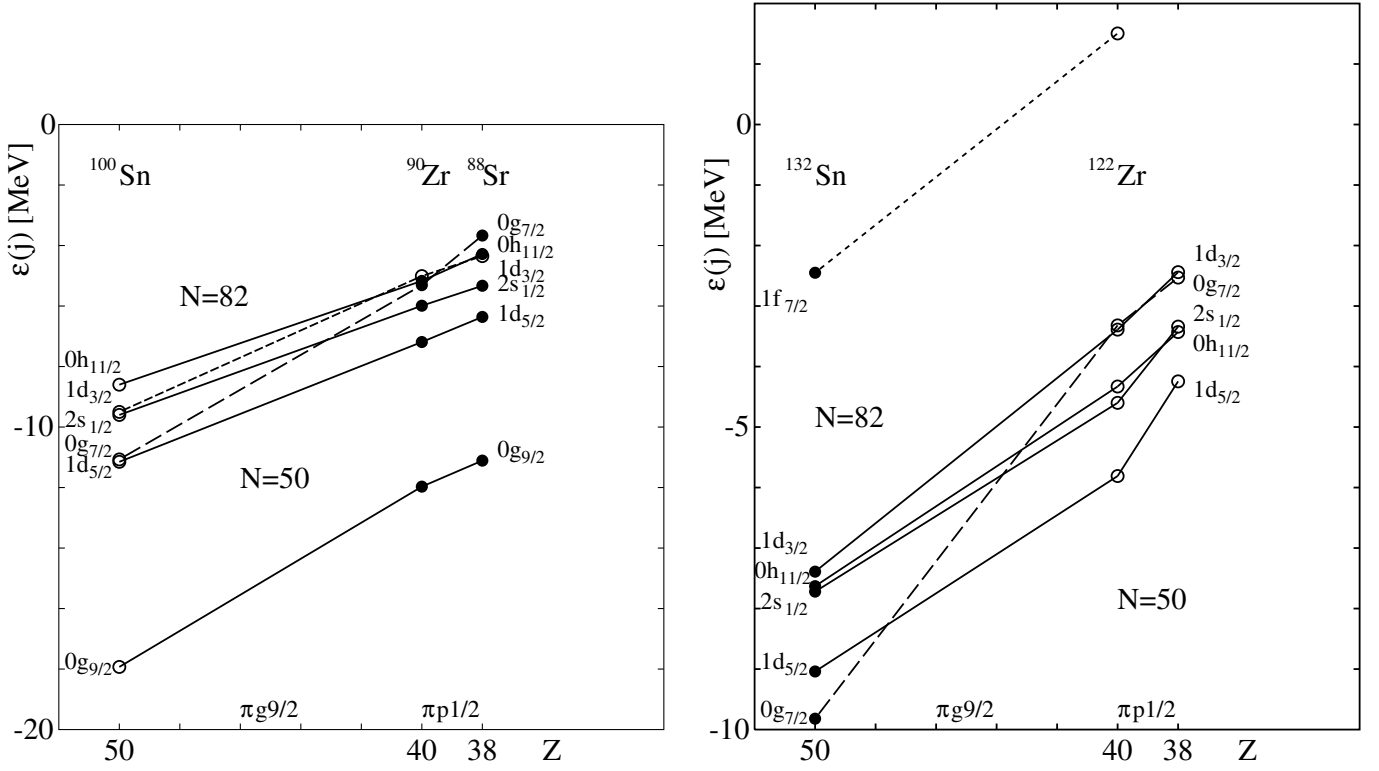
Fig. 8. Shell evolution along $N = 50$ (left) and $N = 82$ (right) isotones with the (MHJ) realistic interaction for ^{88}Sr and ^{100}Sn core, respectively. The interactions for the $\nu g_{9/2}$ orbit below $N = 50$ is from an empirical fit [7,23] and for the $\nu f_{7/2}$ orbit above $N = 82$ from extrapolation from the ^{208}Pb region [6].

sequence in ^{101}Sn (see fig. 4); ii) it calculates the excitation energy of the $I^\pi = 1/2^-$ isomer in ^{103}In much too high relative to the $I^\pi = 9/2^+$ ground state [51]. These excitation energies are shown in the lower panel of fig. 9. Both deficiencies can be cured by tuning the $\pi g_{9/2}$-$\nu g_{7/2}$ and $\pi p_{1/2}$-$\nu d_{5/2}$ monopoles. The results for the shell gap are shown by full lines in the upper panel and by a full line circle in the lower panel next to the experimental ^{103}In point (SM). Due to lacking experimental information the monopoles involving the $\pi p_{3/2}, f_{5/2}$ were not corrected. The features of the $Z = 40$ shell extrapolation are summarised as follows:

– In spite of the qualitative character of the extrapolation by using eq. (2) instead of an involved shell model calculation, the experimental shell gap is well reproduced. Especially the stabilisation from ^{90}Zr ($N = 50$) to ^{96}Zr ($N = 56$) and the following quenching towards the strongly deformed region $^{100-104}$Zr is accounted for.

– Beyond $N = 64$ upon filling of the $\nu 2s_{1/2}, 0h_{11/2}, 1d_{3/2}$ orbitals the gap is widening again to reach ~ 4.35 MeV at $N = 82$, which has to be compared to 3.198 MeV and 4.036 MeV at $N = 50$ and 56, respectively. The $N = 82$ (^{122}Zr) value is an upper limit, as the interaction derived for ^{88}Sr was not scaled by $A^{-1/3}$ which yields a 10% reduction. The weakness of this extrapolation is the lack of any experimental verification.

– Exploiting the above-mentioned sensitivity of the excitation energy of the $I^\pi = 1/2^-$ isomer in ^{103}In to the

tuning of the interaction, in the lower panel of fig. 9 these excitation energies are shown for all In isotopes. A clear correlation of this energy with the width of the shell gap is seen up to $N = 64$. Beyond the minimum at $N \sim 64$ the values are rising again as predicted by the shell gap extrapolation. The trend is stopped, however, at $N = 78$ which casts some doubt on the predicted persistence of the $Z = 40$ shell gap. It should be noted though that the last three points are results of β-endpoint mass measurements. Recent mass measurements using ion traps in neutron-rich Sr-Ru isotopes revealed up to ~ 1 MeV discrepancies as compared to β-endpoint results [52].

– We note in passing that the $Z = 40$ shell gap extrapolation including the trend in the In probe does not show any sign of double-magicity for the $Z = 40$, $N = 70$ nucleus ^{110}Zr.

In conclusion the persistence of the $Z = 40$ gap at $N = 82$ is still an open question. So a possible quenching of the $N = 82$ gap may find a simple explanation in the lack of the $Z = 40$ gap, which would make ^{122}Zr a mid-shell nucleus with reduced neutron gap due to *ph* excitations across the shell.

An alternative scenario for filling the abundance trough below $A \simeq 130$ is based on the steep upsloping of the $\nu g_{7/2}$ level from the deepest in the shell at ^{132}Sn to the Fermi surface at ^{122}Zr as shown in fig. 8 right panel. The allowed GT transition is delayed as the $\nu 0g_{7/2}$ starts to be filled only about 12 nucleons below $N = 82$ thus
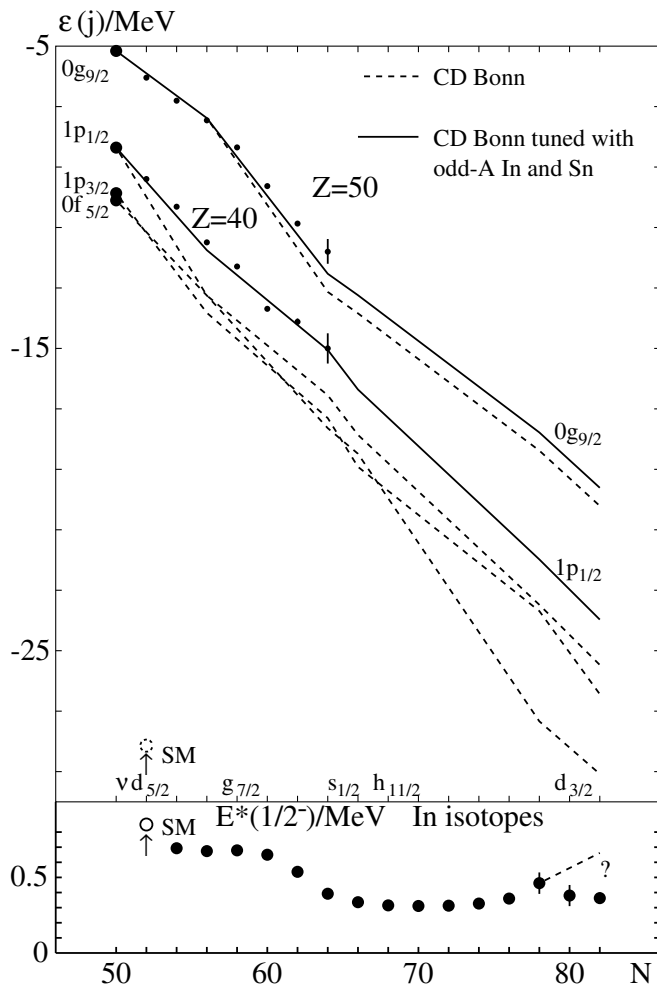
Fig. 9. Evolution of the $Z = 40$ shell gap (top panel) and the splitting of the $I^\pi = 9/2^+$ g.s. and $I^\pi = 1/2^-$ isomer in In isotopes.

increasing β-decay halflives in the region $A < 130$. On the other hand a filled $\nu 0g_{7/2}$ orbit at $N \sim 82$ at the Fermi surface causes large effective Q_β values, which decreases the halflives in this region. As a consequence the abundance peak intensities will be shifted to lighter masses. This scenario, however, neglects the influence of neutron separation energies, which in case of a quenched shell are inherently included.

6 Summary and conclusions

It has been shown that isomer decay spectroscopy close to magic nuclei provides a very sensitive probe of residual interactions and single particle energies employed in shell model calculations. The strong proton-neutron interaction in identical orbitals at $N = Z$ gives rise to spin-gap isomers exhibiting exotic decay modes such as p and 2p decay. An indispensable prerequisite for sound predictions are readily available large scale shell model codes along with realistic interactions that in their monopole part are well adjusted to experimental single particle energies. This

does not necessarily hamper the predictive power of shell model calculations as the tuning can be done in regions accessible to detailed spectroscopy (see sects. 2 and 5). Monopole driven shell evolution can account for many aspects of structural changes on the pathway from proton-rich $N \sim Z$ nuclei (^{100}Sn) to the neutron-rich $N \gg Z$ (^{78}Ni) region. The concept has been shown to account for the new shell closures established in light nuclei, shell reordering and evolution of spin-orbit splitting in medium-heavy nuclei, and it provides an alternative access to the structure of $N \gg Z$ r-path nuclei.

References

1. A. Bohr, B.R. Mottelson, *Nuclear Structure* (World Scientific, Singapore 1998).
2. J. Dobaczewski *et al.*, Phys. Rev. Lett. **72**, 981 (1994).
3. T. Otsuka *et al.*, Phys. Rev. Lett. **87**, 0852502 (2002).
4. T. Otsuka *et al.*, Acta Phys. Pol. B **36**, 1213 (2005); Phys. Rev. Lett. **95**, 232502 (2005).
5. H. Grawe, Acta Phys. Pol. B **34**, 2267 (2003).
6. H. Grawe *et al.*, Eur. Phys. J. A **25**, s01, 357 (2005).
7. H. Grawe *et al.*, Physica Scripta T **56**, 71 (1995).
8. H. Grawe, M. Lewitowicz, Nucl. Phys. A **693**, 116 (2001).
9. H. Grawe, Springer Lect. Notes Phys. **651**, 33 (2004).
10. A. Blazhev *et al.*, Phys. Rev. C **69**, 064304 (2004).
11. C. Plettner *et al.*, Nucl. Phys. A **733**, 20 (2004).
12. R. Grzywacz *et al.*, Phys. Rev. C **55**, 1126 (1997).
13. M. Górska *et al.*, Z. Physik A **353**, 233 (1995).
14. E. Nolte, H. Hicks, Phys. Lett. B **97**, 55 (1980).
15. J. Döring *et al.*, GSI Ann. Rep. (2003) and to be published.
16. J. Döring *et al.*, Phys. Rev. C **68**, 034306 (2003).
17. K. Ogawa, Phys. Rev. C **28**, 958 (1983).
18. M. Górska *et al.*, *Proceedings of the 8th International Spring Seminar on Nuclear Physics, Key Topics in Nuclear Structure, Paestum, Italy, 2004*, edited by A. Covello (World Scientific, Singapore, 2005) p. 229.
19. M. Górska *et al.*, Phys. Rev. Lett. **79**, 2415 (1997).
20. I. Mukha *et al.*, Phys. Rev. C **70**, 044311 (2004).
21. I. Mukha *et al.*, Phys. Rev. Lett. **95**, 022501 (2005).
22. I. Mukha *et al.*, Nature **439**, 298 (2006).
23. M. Górska *et al.*, ENPE99, AIP Conf. Proc. **495**, 217 (1999).
24. M. Hjorth-Jensen *et al.*, Phys. Rep. **261**, 125 (1995) and private communication.
25. T. Otsuka *et al.*, Eur. Phys. J. A **15**, 151 (2002).
26. T. Motobayashi *et al.*, Phys. Lett. B **346**, 9 (1995).
27. M. Hanawald *et al.*, Phys. Rev. Lett. **82**, 1391 (1999).
28. J.P. Schiffer *et al.*, Phys. Rev. Lett. **92**, 162501 (2004).
29. O. Sorlin *et al.*, Phys. Rev. Lett. **88**, 092501 (2002).
30. K.H. Langanke *et al.*, Phys. Rev. C **67**, 044314 (2003).
31. M. Sawicka *et al.*, Eur. Phys. J. A **16**, 51 (2002).
32. A. Bürger *et al.*, Phys. Lett. B **622**, 29 (2005).
33. D.-C. Dinca *et al.*, Phys. Rev. C **71**, 041302 (2005).
34. R.V.F. Janssens, *et al.*, Phys. Lett. B **546**, 55 (2002).
35. K.-L. Kratz *et al.*, Phys. Rev. C **38**, 278 (1988).
36. Y.H. Zhang *et al.*, Phys. Rev. C **70**, 024301 (2004).

37. R. Grzywacz *et al.*, Phys. Rev. Lett. **81**, 766 (1998).
38. J.M. Daugas *et al.*, Phys. Lett. B **476** 213 (2000).
39. M. Sawicka *et al.*, Eur. Phys. J. A **20**, 109 (2004).
40. R. Grzywacz, Eur. Phys. J. A **25**, s01, 89 (2005).
41. S. Franchoo *et al.*, Phys. Rev. C **64**, 054308 (2001).
42. A. Lisetskiy *et al.*, Eur. Phys. J. A **25**, s01, 95 (2005).
43. H. Grawe *et al.*, Nucl. Phys. A **704**, 211c (2002).
44. M. Sawicka *et al.*, Phys. Rev. C **68**, 044304 (2003).
45. O. Perru *et al.*, submitted to Phys. Rev. Lett.
46. H. Mach *et al.*, *Proceedings of the International Symposium A New Era of Nuclear Structure Physics, Niigata, Japan 2003*, edited by Y. Suzuki, S. Ohya, M. Matsuo, T. Ohtsubo (World Scientific, Singapore, 2004) p. 277.
47. H. Mach *et al.*, to be published.
48. B. Pfeiffer *et al.*, Nucl. Phys. A **693**, 282 (2001).
49. I. Dillmann *et al.*, Phys. Rev. Lett. **91**, 162503 (2003).
50. T. Kautzsch *et al.*, Eur. Phys. J. A **9**, 201 (2000).
51. O. Kavatsyuk *et al.*, Eur. Phys. J. A **25**, 211 (2005).
52. J. Äystö, these proceedings.